ISSN: 0369-8963

Effects of Magnetic Field and Ohmic Heating on Mixed Convection over a Vertical Heated Plate

Sowmya S B[1*], Nalinakshi N[2], Sreenivasa T N[3]
[1]Department of Mathematics, Government Science College, Nrupathunga University Bengaluru-560001, KA, India
[2]Department of Mathematics, Atria Institute of Technology, Bengaluru-560024, KA, India.
[3]Department of Mechanical Engineering, Atria Institute of Technology, Bengaluru-560024, KA, India.

ABSTRACT

The purpose of this study is to investigate the synergistic impacts of external magnetic fields (MHD) and ohmic heating on mixed convection phenomena occurring over a vertical heated plate situated within a porous medium, in conjunction with analyzing the implications of internal heat generation (IHG). The presence of convective boundary layer flows in Cu-H2O nanofluids is essential for comprehending the flow characteristics of various physical systems and practical applications. such as semiconductor wafers, electronic chips, thermal insulation, and nuclear reactors. This work utilizes a Bvp4c method to solve the governing nonlinear differential equations. In this study, the effects of MHD, ohmic, radiation on the flow characteristics and thermal transfer of the different nanoparticles are investigated. The results show that the velocity profile increases with increasing solid volume fraction, heat absorption, and magnetic parameter but the opposite trend is observed in the temperature profile with increasing volume fraction and heat generation as observed in both UP and VP cases. For all radiation parameter values, the Nusselt number increases with the Grashof number due to enhanced buoyancy-driven heat transfer.

Key Words: Mixed convection, Nanofluids, Variable fluid properties, Radiation, Ohmic effect.

1. INTRODUCTION

In the present century, marked by the rapid advancement of technological innovations, there exists a considerable demand for fluids that demonstrate high thermal conductivity. To tackle the challenges arising from insufficient conductivity, researchers are necessitated to develop fluids that exhibit improved thermal conductivities. The groundbreaking work of Choi and Eastman [1] led to the introduction of the concept of ‘nano-fluid’, which pertains to fluids infused with suspended nanoparticles. These fluids manifest distinctive and superior thermophysical characteristics. Choi et al.[2] undertook practical investigations that demonstrated how even minor amounts of nanoparticles incorporated into standard fluids can significantly affect their thermal conductivity properties. In the wake of this promising investigation, a multitude of researchers, including Wang et al. [3], Das et

 https://doi.org/10.5281/zenodo.14227176

al. [4], and Kakac and Pramuanjaroenkij [5], have undertaken studies on the dynamics of nano-fluids to attain a more thorough comprehension of the phenomenon.

In the previously mentioned studies, the viscosity, porosity, permeability, and thermal conductivity of nanofluids are presumed to remain constant. In particular, the dynamic viscosity and thermal conductivity of the nanofluid are considered to remain constant. It is an established understanding that fluid characteristics may change with temperature; therefore, to effectively anticipate the flow, heat, and mass transfer attributes of the fluid, it is crucial to regard viscosity and thermal conductivity as variables dependent on temperature. In this examination, we have characterized the working fluid as the nanofluid. A review of the existing literature surrounding nanofluids uncovers that both the viscosity and thermal conductivity are variable and show considerable shifts as temperature varies [4, 6]. Khanafer and Vafai [7] performed both theoretical and experimental investigations to evaluate the effects of variable viscosity and thermal conductivity in nanofluids.

The significance of internal heat generation is crucial for comprehending the flow characteristics of various physical systems and practical applications such as semiconductor wafers, electronic chips, and nuclear reactors. Specifically, the effect of heat generation predominantly influences the temperature distribution rather than the velocity and concentration profiles. Furthermore, the examination of convective boundary layer flows with internal heat generation (IHG) on a vertical porous flat plate has garnered substantial interest for a range of industrial and practical uses, including the cooling of rocket engines, nuclear reactors, combustion chambers, thermal insulation, and geothermal reservoirs.

Gasser and Kazimi [8] examined how internal heat generation influences the instability of convective flow in a porous medium. Moalem [9] analyzed the variations in temperature distribution instigated by heat generation in a steady-state convective flow through a porous structure. In their study, Vajravelu [10] looked into the combined influences of internal heat generation and variable fluid properties on natural convective flow along a heated vertical surface in an air setting. The occurrence of mixed convection from a vertically aligned plate subjected to convective heating, interacting with a fluid that has internal heat generation, has been analyzed by Makinde and Aziz [11]. Chandrasekhar and Namboodiri [12] highlighted the significance of the variable permeability of the porous medium on heat transfer and velocity distribution. Uniform permeability significantly affects velocity and temperature profiles more than variable permeability does. This aspect is vital when creating microfluidic heat sinks for cooling electronic devices.

The significant effects of internal heat generation cause the plate's surface temperature to exceed the fluid temperature at the bottom boundary, leading to a reversal in heat transfer as noted by Olanrewaju et al. [13]. Nalinakshi et al. [14-15] conducted a numerical study examining the effects of internal heat generation on mixed convective flow over a vertically aligned heated flat plate, using the shooting method while accounting for variable fluid properties.

The presence of mixed convection in Cu-H2O nanofluids is essential for understanding the influences of thermal radiation, Ohmic heating, heat generation, and magnetohydrodynamics (MHD), which are common in numerous technical applications such as cooling systems and energy conversion devices. Furthermore, many researchers have shown a keen interest in investigating

 https://doi.org/10.5281/zenodo.14227176

MHD flow in conjunction with mass transfer through porous media, as this has considerable consequences for various industrial activities, including the annealing and tinning of copper wires, as well as metallurgical processes like the continuous drawing of filaments through stagnant fluids. The improvement of heat transfer in mixed convection scenarios using Cu-H2O nanofluids under the operational conditions of nuclear reactors was studied by Buongiorno and Hu [16]. The findings reveal that incorporating Cu nanoparticles greatly boosts heat transfer, thus enhancing cooling performance. Sheikholeslami et al. [17] investigate the relationship between magnetohydrodynamics (MHD) and forced convection flow across a vertical surface. Their study is augmented by the incorporation of a Cu-H2O nanofluid to assess the impacts of magnetohydrodynamics, thermal generation, radiation, and chemical interactions on the flow dynamics and thermal transfer efficiency of the nanofluid (specifically Cu-H2O) on a vertical plate. The research conducted by Sheikholeslami and Shafii [18] elucidates the alterations in velocity and temperature profiles induced by the magnetic field. Recently, Hari Krishna et al. [19] focused on the synergistic effects of thermal radiation and chemical reactions on MHD mixed convective flow, emphasizing the critical role of Joule heating and viscous dissipation.

A porous structure facilitates the enhanced integration of the nanofluid, leading to a uniform temperature distribution and preventing the formation of localized hot spots. This quality holds great importance in industrial situations, where ensuring a reliable temperature is vital for the standard of the final output and the operational productivity. The analysis by Padma et al. [20] reveals the key significance of thermal transfer in Cu-H2O nanofluids for uses that demand efficient cooling solutions, particularly in electronic devices and heat exchangers. Additionally, Xin and colleagues [21] observed a notable increase in temperature corresponding to heightened thermal radiation levels, suggesting that Cu-H2O nanofluids are capable of effectively handling heat in scenarios involving high thermal loads, such as thermal treatment systems and medical imaging equipment. In conclusion, the interaction between thermal radiation and viscous dissipation in Cu-H2O nanofluids within porous media improves heat transfer, stability, and fluid dynamics regulation. This makes the solution both efficient and adaptable for a variety of industrial and medical applications, as explored in the literature review by Matao et al. [22], Basant and Gabriel [23,24], and Madhura et al. [25].

The primary aim of the current study is to explore and evaluate the combined effects of external magnetic fields (MHD) and ohmic heating on mixed convection behaviors occurring over a vertical plate placed within a porous medium, while also examining the effects of internal heat generation. This investigation will encompass a comprehensive assessment of different fluid traits, namely porosity and permeability, along with the flow mechanics and thermal exchange in nanofluids. This study aims to reveal how shifts in the power and orientation of the magnetic field, together with the attributes of the nanofluid, shape the complete efficiency of heat transfer. This research intends to improve the performance of thermal management systems across various engineering domains by probing the potential advantages of employing MHD and ohmic heating to enhance and regulate heat transfer processes.

 https://doi.org/10.5281/zenodo.14227176

2. MATHEMATICAL FORMULATION

Consider a steady, incompressible, laminar, two-dimensional mixed convection boundary layer and electrically conductive viscous fluid undergoing mixed convection over a vertical plate while accounting for thermal radiation under the influence of internal heat generation and viscous dissipation for the Forchheimer model. Variations in the permeability and porosity of the fluid flow must be addressed. The physical model's coordinate system is demonstrated in Figure 1. In the arrangement of the flow, the vertical plate remains secured along the x-axis, while it is considered that the fluid ascends along the plate, with the y-axis aligned precisely at a right angle to the plate. Additionally, it is assumed that the plate is maintained at a constant uniform temperature T_w and concentration C_w, both of which surpass T_∞ and C_∞, respectively. A uniform free stream velocity U_0 is presumed to be constant. A uniform magnetic field of strength B_0 is applied perpendicular to the plate, and the induced magnetic field resulting from the motion of the electrically conductive fluid is regarded as negligible. Under these assumptions and employing the theory of boundary layer approximations, the governing equations are derived as follows [26]:

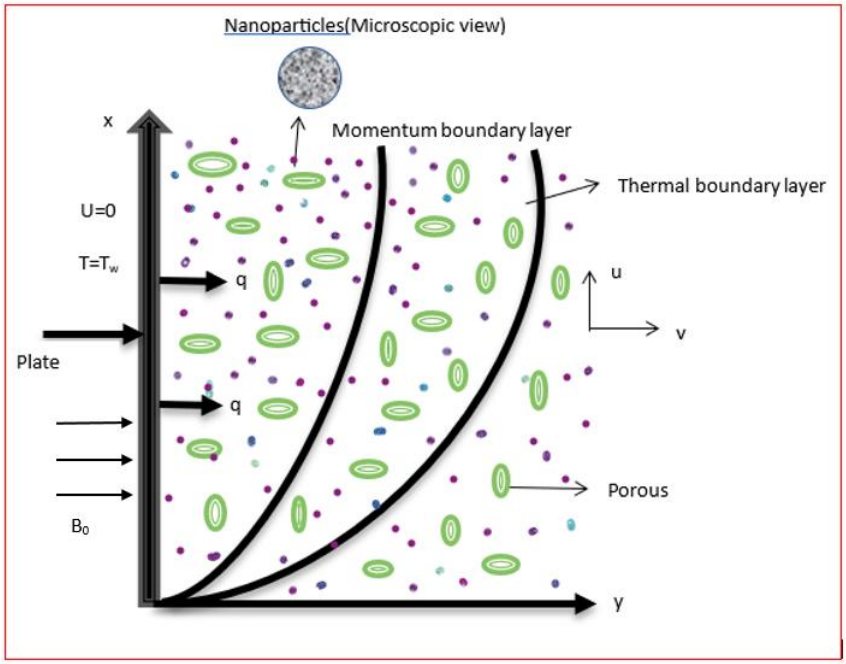

Figure 1: Physical configuration of the system

Conservation of Mass,

$$\frac{\partial u}{\partial x}+\frac{\partial u}{\partial y}=0 \tag{1}$$

Momentum Equation,

$$\rho_{nf}\left(u\frac{\partial u}{\partial x}+v\frac{\partial u}{\partial y}\right)=g\left(\rho\beta\right)_{nf}\left(T-T_\infty\right)+\mu_{nf}\frac{\partial^2 u}{\partial y^2}+\frac{\mu_{nf}}{k(y)}\varepsilon(y)\left(U_0-u\right)+\frac{F\varepsilon^2(y)}{\sqrt{k(y)}}\left(U_0{}^2-u^2\right)-\sigma_{nf}B_0{}^2u \tag{2}$$

Energy Equation,

 https://doi.org/10.5281/zenodo.14227176

ISSN: 0369-8963

$$\left(\rho c_p\right)_{nf}\left(u\frac{\partial T}{\partial x}+v\frac{\partial T}{\partial y}\right)=K_{nf}\frac{\partial^2 T}{\partial y^2}-\frac{\partial q_r}{\partial y}+\mu_{nf}\left(\frac{\partial u}{\partial y}\right)^2+\sigma_{nf}B_0^2u^2-Q_0\left(T-T_\infty\right) \tag{3}$$

The above governing equations need to be solved subject to the boundary conditions,

$$u=0,\ v=0,\ T=T_w \text{ at y=0} \tag{4}$$

$$u=U_0,\ \text{v=0},\ T=T_\infty \text{ as } y\to\infty \tag{5}$$

The correlation between the nanofluid and the fluid [27].

$$\begin{aligned}&\alpha_{nf}=\frac{K_{nf}}{\left(\rho c_p\right)_{nf}},\ \rho_{nf}=\left(1-\phi\right)\rho_f+\phi\rho_s\\&\frac{K_{nf}}{K_f}=\frac{\left(K_s+2K_f\right)-2\phi\left(K_f-K_s\right)}{\left(K_s+2K_f\right)+2\phi\left(Kf-K_s\right)},\mu_{nf}=\frac{\mu_f}{\left(1-\phi\right)^{2.5}}\end{aligned} \tag{6}$$

The radiative heat flux can be written by using the Rosseland approximation given by [28],

$$q_r=-\frac{4\sigma^*}{3k^*}\frac{\partial T^4}{\partial y} \tag{7}$$

Where, σ^* the Stefan Boltzmann constant and the Rosseland mean observation co-efficient is k^*. Now by assuming a modest temperature difference with the flow and by using the Taylor series to expand the T^4 and T_∞ where the temperature may be stated as a linear function of temperature as shown in the following equation,

$$T^4=T_\infty^4+4T_\infty^3\left(T-T_\infty\right)+6T_\infty^2\left(T-T_\infty\right)^2+\text{L}$$

Ignoring higher-order terms in the above equation beyond the first-order $\left(T-T_\infty\right)$, we get

$$T^4\cong 4TT_\infty^3-3T_\infty^4 \tag{8}$$

On Substituting equation (7) into equation (6) we get

$$\frac{\partial q_r}{\partial y}=-\frac{16\sigma T_\infty^3}{3k^*}\frac{\partial^2 T}{\partial y^2} \tag{9}$$

The Eq. (3) will be reduced to the form:

$$\left(\rho c_p\right)_{nf}\left(u\frac{\partial T}{\partial x}+v\frac{\partial T}{\partial y}\right)=\kappa_{nf}\frac{\partial^2 T}{\partial y^2}+\frac{16\sigma T_\infty^3}{3k^*}\frac{\partial^2 T}{\partial y^2}+\mu_{nf}\left(\frac{\partial u}{\partial y}\right)^2+\sigma_{nf}B_0^2u^2-Q_0\left(T-T_\infty\right) \tag{10}$$

We now introduce the following dimensionless variables f and θ as well as similarity variable η.

$$\eta=\left(\frac{y}{x}\right)\left(\frac{U_0x}{\gamma}\right)^{\frac{1}{2}},\ \psi=\sqrt{\gamma U_0x}\,f\left(\eta\right),\ \theta=\frac{T-T_\infty}{T_w-T_\infty} \tag{11}$$

Where a prime represents differentiation concerning η and $T=T_w$ is the plate temperature.

In equation (11) the stream function $\psi\left(x,y\right)$ is defined, such that the

 https://doi.org/10.5281/zenodo.14227176

ISSN: 0369-8963

continuity equation (1) is satisfied automatically and the velocity components are given by,

$$u = U_0 f'(\eta),\ v = -\frac{1}{2}\sqrt{\frac{\upsilon U_0}{x}}\left(f(\eta) - \eta f'(\eta)\right) \tag{12}$$

The Variable porosity $\varepsilon(\eta)$ and the variable permeability $k(\eta)$ are given by,

$$\varepsilon(\eta) = \varepsilon_0\left(1 + d^* e^{-\eta}\right) \tag{13}$$

$$k(\eta) = k_0\left(1 + de^{-\eta}\right) \tag{14}$$

Where ε_0, k_0 have been the porosity and the permeability at the boundary layer edge correspondingly, d and d^* which have been the constants whose values have been considered as 3.0 & 1.5 [29].

Substituting Eq. (11), (12)-(14) in Eqs. (2) & (10), We obtain the transformed equations as follows.

$$f''' + \frac{A_1 A_2}{2} ff'' + \frac{Gr}{\mathrm{Re}^2}\theta A_1 A_2 + \frac{(1 - f')\left(1 + d^* e^{-\eta}\right)}{\mathrm{Re}\, K\left(1 + de^{-\eta}\right)} + \frac{\beta^*\left(1 + d^* e^{-\eta}\right)^2\left(1 - f'^2\right)}{\left(1 + de^{-\eta}\right)^{1/2}} A_1 - M^2 A_1 A_5 f' = 0 \tag{15}$$

$$2A_1\left(A_4 + R\right)\theta'' + Ec\,\mathrm{Pr}\, f''^2 + A_1 A_3\,\mathrm{Pr}\, f\theta' + 2A_1 A_5\,\mathrm{Pr}\, EcM^2 f'^2 - 2A_1\,\mathrm{Pr}\, Q\theta = 0 \tag{16}$$

Were,

$Gr = \dfrac{g\beta_f\left(T_w - T_\infty\right)\nu_f}{U_0^3}$ is the Grashof number

$\mathrm{Pr} = \dfrac{\left(\mu c_p\right)_f}{k_f}$ Prandtl number

$R = \dfrac{4\sigma^* T_\infty^3}{k^* k_f}$ radiation parameter

$Ec = \dfrac{U_0^2}{\left(c_p\right)_f\left(T_w - T_\infty\right)}$ the Eckert no.

$\mathrm{Re} = \dfrac{U_0 x}{\nu_f}$ Reynold's No.

$M^2 = \dfrac{\sigma B_0^2 x}{U_0 \rho_f}$ Magnetic term

$\beta^* = \dfrac{F\varepsilon_0^2 x}{k_0^{1/2}}$ Inertial parameter

$Q = \dfrac{Q_0 x}{U_0^2\left(\rho C_p\right)_f}$ Internal Heat source/sink

The Transformed boundary conditions are:

$$f = 0,\ f' = 0,\ \theta = 1 \text{ at } \eta = 0 \tag{17}$$

$$f' = 1,\ \theta = 0 \text{ as } \eta \to \infty \tag{18}$$

 https://doi.org/10.5281/zenodo.14227176

ISSN: 0369-8963

Where,

$$A_1 = (1-\phi)^{2.5},\ A_2 = (1-\phi) + \phi\left(\frac{\rho_s}{\rho_f}\right)$$

$$A_3 = (1-\phi) + \phi\frac{(\rho c_p)_s}{(\rho c_p)_f},\ A_4 = \frac{\kappa_s + 2\kappa_f - 2\phi(\kappa_f - \kappa_s)}{\kappa_s + 2\kappa_f + \phi(\kappa_f - \kappa_s)}$$

$$A_5 = 1 + \frac{3(\sigma-1)\phi}{(\sigma+2) - (\sigma-1)\phi}$$

Skin-friction:

The dimensionless skin friction takes the following forms based on the velocity field:

$$c_{fx} = -A_1\frac{f''(0)}{\sqrt{\mathrm{Re}}} \tag{19}$$

Nusselt Number:

We examine the dimensionless Nusselt number from the temperature field in the following ways:

$$N_{ux} = -\left(\frac{k_{nf}}{k_f} + R\right)\sqrt{\mathrm{Re}}\,\theta'(0) \tag{20}$$

Table 1. Thermophysical properties of water and nanoparticles[30]

Physical Properties	Water/base fluid	Cu(Copper)
ρ, kg/m^3	997.1	8933
c_p, $J/kg\ \ K$	4179	385
k, $W/m\ \ K$	0.613	401
σ, S/m	0.05	59.6×10^6

3. METHOD OF SOLUTION

The boundary value problems represented by equations (15) and (16) display notable nonlinearity, corresponding to the 3rd and 2nd orders, respectively. The non-linear BVP (Boundary Value Problem) is approached through the Shooting method. The intricate non-linear BVP, which comprises 3rd-order and 2nd-order equations, is subsequently transformed into a system of five simultaneous first-order equations featuring five unknowns.

$$f_1' = f_2,\ f_2' = f_3$$

https://doi.org/10.5281/zenodo.14227176

ISSN: 0369-8963

$$f_3' = -\left(\frac{A_1 A_2}{2} f_1 f_3 + \frac{Gr}{R_e^{\,2}} f_4 A_1 A_2 + \frac{(1-f_2)\left(1+d^* e^{-\eta}\right)}{R_e K \left(1+de^{-\eta}\right)} + \frac{\beta^* \left(1+d^* e^{-\eta}\right)^2 \left(1-f_2^2\right)}{\left(1+de^{-\eta}\right)^{1/2}} A_1 - M^2 A_1 A_5 f_2 \right) \quad (21)$$

$$f_4' = f_5$$

$$f_5' = -\left(\frac{1}{2} \Pr f_1 f_5 \frac{A_3}{\left(A_4+R\right)} + Ec \Pr f_3^{\,2} \frac{1}{\left(A_4+R\right) A_1} + A_5 f_2^{\,2} EcM^2 \Pr \frac{1}{\left(A_4+R\right)} - Q \Pr f_4 \frac{1}{\left(A_4+R\right)} \right) \quad (22)$$

Where $f_1 = f,\ f_2 = f',\ f_3 = f'',\ f_4 = \theta,\ f_5 = \theta'$ and a prime represents the differentiation concerning η . Now, the boundary conditions ;

$$f_1 = 0,\ f_2 = 0,\ f_4 = 1 \quad \text{at} \quad \eta = 0 \quad (23)$$

$$f_2 = 1,\ f_4 = 0 \quad \text{as} \quad \eta \to \infty \quad (24)$$

4. RESULTS AND DISCUSSIONS

The present work employs varying fluid parameters and nanofluids to examine the phenomenon of mixed convection over a vertically heated plate. The complicated system of governing equations is composed of strong interdependencies and non-linear partial differential equations. The utilization of similarity transformations helps in altering the equations into higher-order ordinary differential equations. Convert higher-order ordinary differential equations into their first-order equivalents, followed by the implementation of the Bvp4c technique.

Specifying the boundary conditions articulated in equations (23) and (24) is paramount for the scholarly investigation. In Table 1, the features of the nanofluid are elaborately discussed. The outcomes of the studies are represented in Figures. 2-16, accompanied by Table 1. The pertinent parameters and thermophysical characteristics of the base fluid (water) and the nanoparticle (copper) are duly considered. The selection of volume fraction adheres to a defined range. The velocity and temperature profiles are exhibited for both uniform permeability (UP) and variable permeability (VP) conditions. The values of d and d^* are postulated as 0 for uniform permeability and 3.0 and 1.5 respectively for variable permeability. Through the incorporation of a base fluid with a nanofluid comprising copper nanoparticles at diverse volume fractions, significant variations are observable in the graphs representing velocity and temperature.

The graphical depiction in Figure 2 shows that adding nanoparticles to a base fluid enhances viscous energy loss and interactions among particles, reducing the fluid's velocity. Under conditions of constant permeability, the resistance to flow is more uniformly distributed, thereby intensifying the influence of nanoparticle concentration on fluid velocity. In scenarios of variable permeability, fluid movement is facilitated even in regions with elevated nanoparticle concentrations, rendering it advantageous for cancer therapy. Nanoparticles improve the precision of drug delivery by adjusting concentration levels and modifying permeability, increasing therapeutic effectiveness and minimizing negative side effects.

The incorporation of Cu nanoparticles in a Cu-H2O nanofluid increases temperature distribution near the boundary layer due to their superior thermal conductivity. The variable

 https://doi.org/10.5281/zenodo.14227176

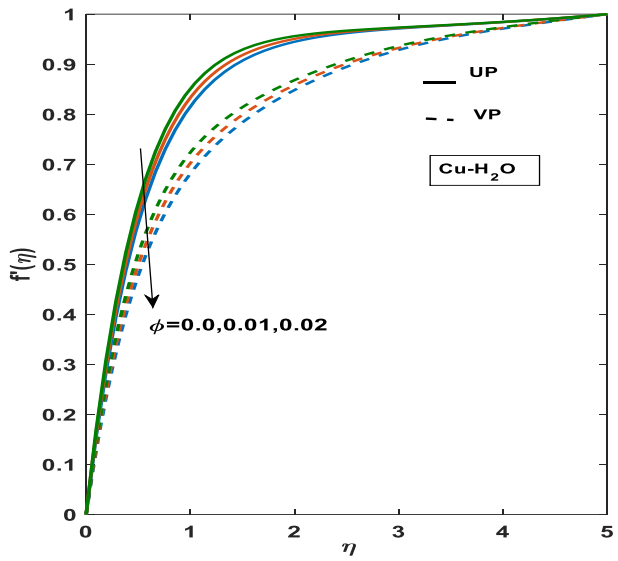

Figure 2: Velocity Profile for various values of ϕ

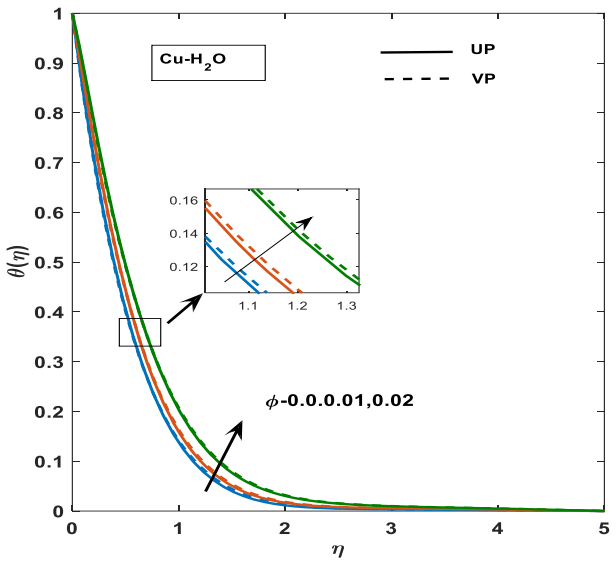

Figure 3: Temperature Profile for various values of ϕ

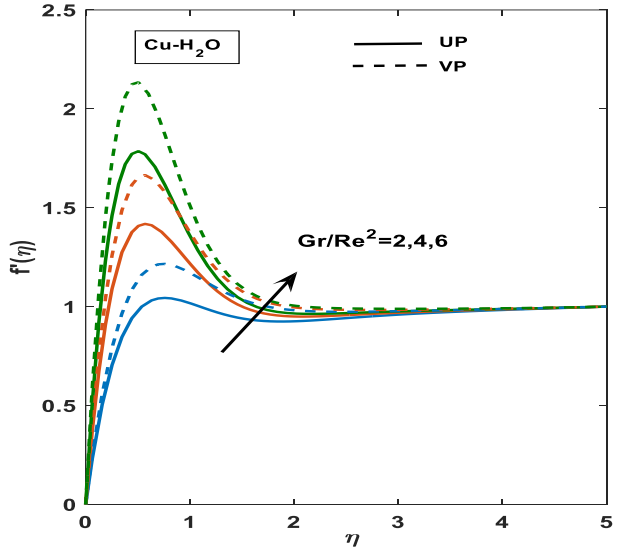

Figure 4: Velocity Profile for various values of Gr/Re^2

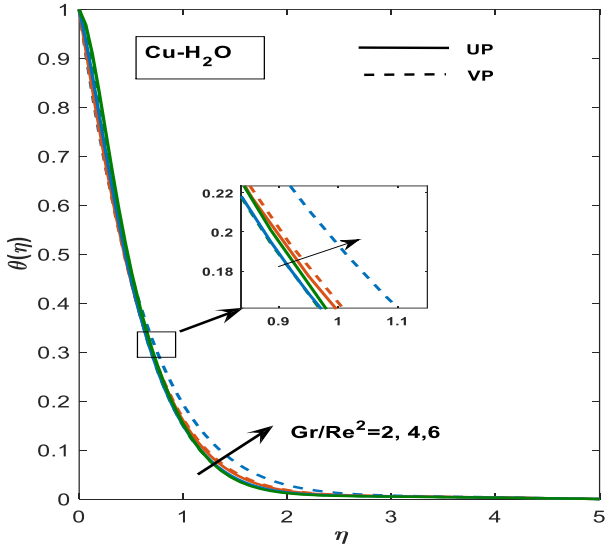

Figure 5: Temperature Profile for various values of Gr/Re^2

permeability (VP) scenario allows for greater control over heat distribution, resulting in slightly higher temperatures near the surface. Copper nanoparticle's heat conduction properties enhance the nanofluid's heat transfer capacity, making them suitable for precise thermal control applications, such as hyperthermia treatment in biomedical engineering as shown in Figure 3.

The examination elucidates the variation in velocity distribution of Cu-H_2O nanofluid flow over a vertical plate, about differing values of the parameters UP and VP. In evaluating the combined flow, the importance of the ratio Gr/Re^2 is underscored for both scenarios, illustrating its comparative significance. An augmentation in the value of Gr/Re^2 markedly improves the velocity distribution in both instances, especially within the boundary layer. Notably, for specific values, of Gr/Re^2 the velocity profile reveals diminished values for VP compared to UP. Moreover, the

https://doi.org/10.5281/zenodo.14227176

boundary layer contracts as the value of Gr/Re^2escalates. The free convection currents generated during the cooling of the plate play a role in increasing the mean velocity. As a result, an escalation in the values of Gr/Re^2tends to enhance buoyancy effects, culminating in intensified induced flow along the vertical plate, as evidenced by the increased fluid velocity illustrated in Figures 4 and 5, which depict the temperature profiles for various increments in the value of $Gr/Re^2$for both UP and VP scenarios. It has been noted that an increase results in a decrease in temperature distribution in both scenarios, indicating that mixed convection with Cu-H_2O nanofluid is optimal for cooling high-performance processors in smartphones.

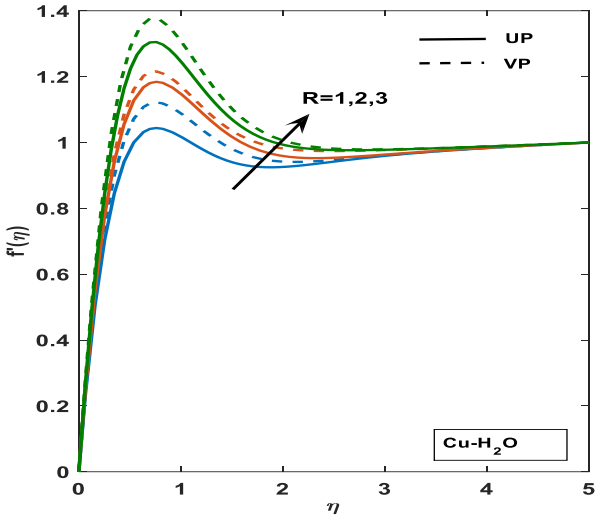

Figure 6: Velocity Profile for various values of R

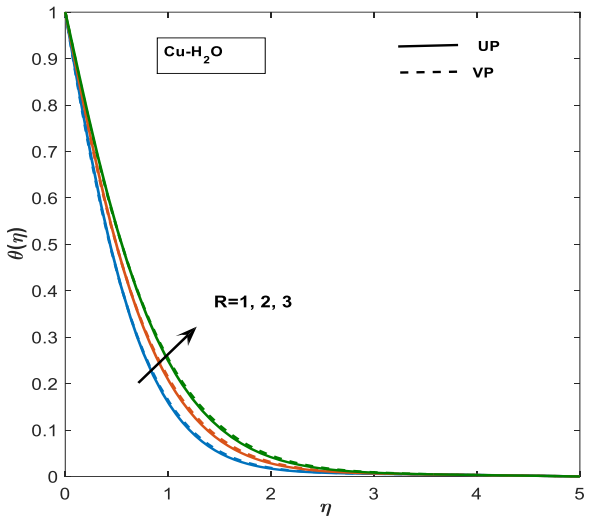

Figure 7: Temperature Profile for various values of R

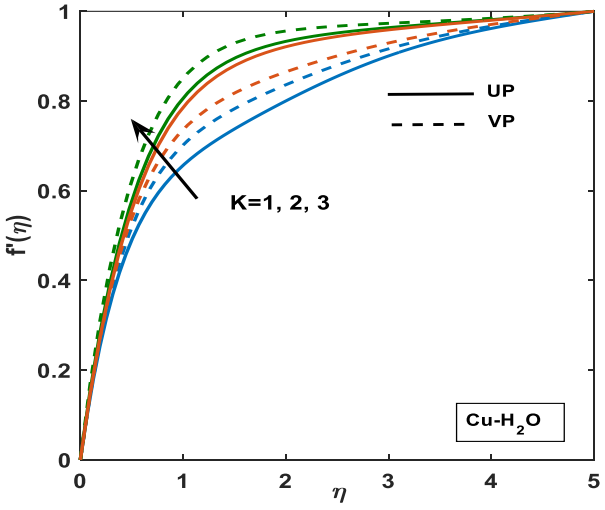

Figure 8: Velocity Profile for various values of K

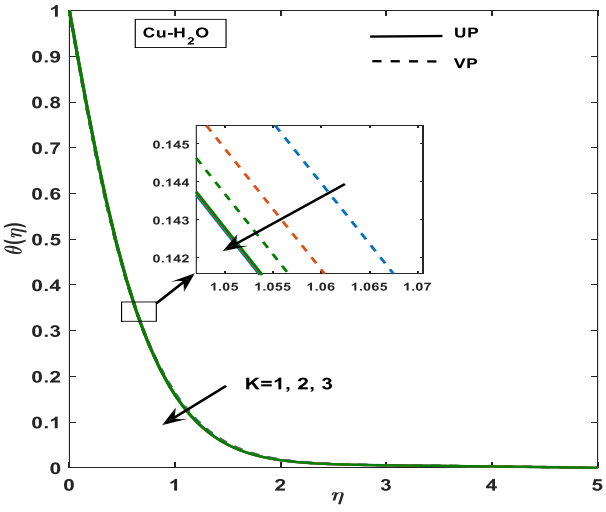

Figure 9: Temperature Profile for various values of K

Figure 6 shows velocity distributions for Cu-water nanofluid, illustrating the enhanced thermal conductivity of the fluid with the incorporation of Cu nanoparticles. This enhances the nanofluid's ability to absorb and disseminate heat, intensifying the buoyancy effect and increasing the velocity profile. The buoyancy-driven acceleration is more pronounced in the VP scenario, where

https://doi.org/10.5281/zenodo.14227176

elevated permeability reduces resistance, resulting in a sharper velocity profile. This configuration allows for controlled heat dissipation, especially in solar collector systems.

Figure 7 shows temperature profiles at different radiation parameter values, showing an increase in temperature with increasing radiation due to higher heat flux, and a monotonic decrease until reaching the free stream temperature, with more significant variation at lower parameters.

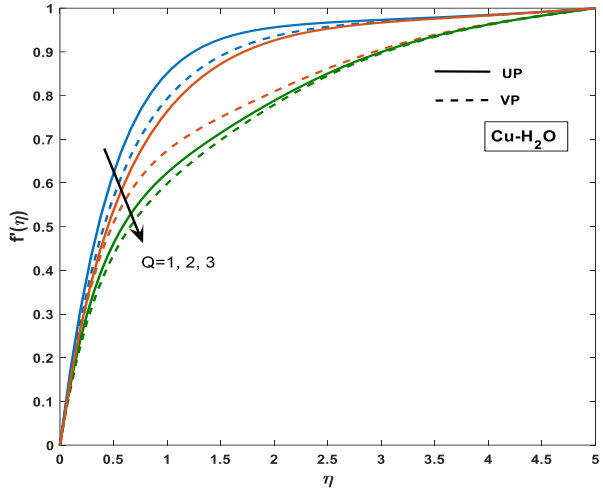

Figure 10: Velocity Profile for various values of Q

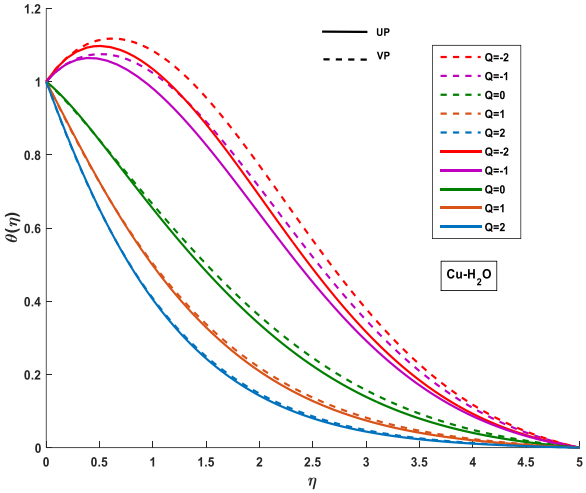

Figure 11: Temperature Profile for various values of Q

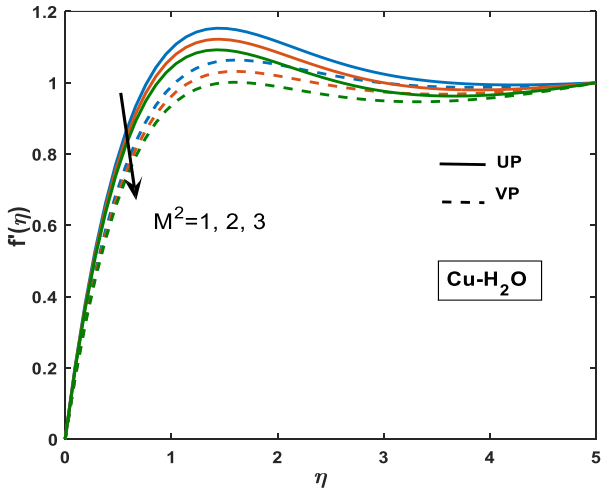

Figure 12: Velocity Profile for various values of M

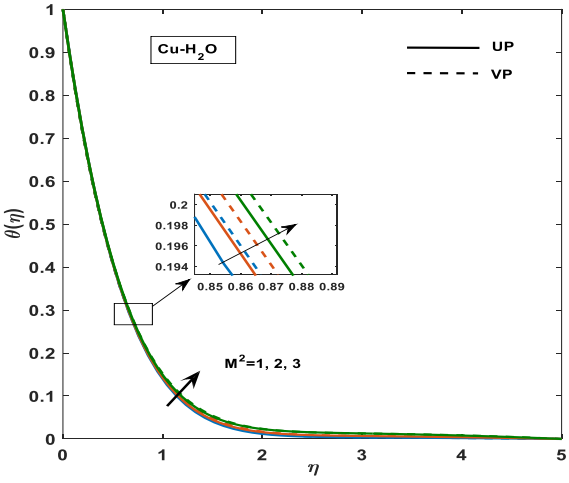

Figure 13: Temperature Profile for various values of M

The graph shows how varying permeability parameters affect the velocity profile of Cu-H_2O nanofluids in both uniform and variable configurations in Figure 8, Variable permeability optimizes flow patterns, reducing fluid resistance and allowing greater adaptability to permeability changes. The inclusion of Cu nanoparticles in H_2O base fluid enhances thermal conductivity, increasing heat transfer efficiency. This is useful for high-performance electronics, such as cooling systems for processors, data centres, or batteries, as it prevents overheating and maintains system stability.

Figure 9 illustrates the effect of varying permeability on the temperature profile of a Cu-H_2O nanofluid near a vertical plate. Higher permeability allows the nanofluid to circulate more

https://doi.org/10.5281/zenodo.14227176

effectively, removing heat from the surface and slightly reducing temperature near the plate. The VP case is more effective at dissipating heat, especially close to the surface, due to variable permeability targeting specific regions for optimized cooling. The combination of high permeability and thermal conductivity aids in efficient cooling.

Figure 10 shows the velocity profile of Cu-H2O nanofluid influenced by heat generation/absorption parameters in uniform permeability (UP) and variable permeability (VP) scenarios. As Q increases, the velocity profile decreases, causing an increase in temperature gradient near the surface and buoyancy forces. However, this also increases fluid viscosity, which opposes flow. The UP scenario shows a gradual decline with distance, while the VP scenario shows a steeper initial decline followed by a gradual reduction. Variable permeability can hinder heat distribution in porous mediums.

Figure 11 shows temperature distributions for Cu-water nanofluid at different heat generation/absorption parameters. The UP and VP examples show an increasing trend in temperature profiles when the heat generation/absorption parameter (Q) rises. The fluid's internal temperature rises due to increased heat generation, while a lower profile results from more heat absorption. The temperature profile decreases when the heat absorption parameter increases, but reverses when heat production increases. The nanofluid's increased heat conduction leads to significant temperature rises in heat production. To improve heat dissipation, electrical equipment uses fans, heat sinks, or microchannel coolers, which generate forced convection for effective heat removal.

Figure 12 shows that Cu-H_2O nanofluid's velocity profile decreases with increasing magnetic parameters due to Lorentz forces. The incorporation of Cu-H_2O nanofluid may also affect flow dynamics, with increased viscosity and thermal conductivity affecting temperature distribution and flow characteristics. Controlling magnetic field strength and medium permeability can improve MHD generator efficiency.

Figure 13 shows the temperature profile of a Cu-H_2O nanofluid over a vertical plate, varying in magnetic parameter M^2. As the magnetic parameter increases, the temperature near the plate slightly decreases. This is due to the Lorentz force induced by the magnetic field, which acts as a resistive force against fluid motion, attenuating convective heat transfer. This reduces flow velocity, reducing convective heat transfer away from the plate and decreasing the overall temperature profile. In the variable permeability case, the fluid moves more freely in regions with higher permeability, promoting more efficient heat dissipation. Applying a magnetic field in nuclear reactors or aerospace components can optimize heat removal by suppressing excessive convective heat transfer, promoting gradual and controlled cooling.

For a range of radiation parameter values, Figure 15 illustrates the relationship between the Nusselt number and the Grashof number Gr/Re^2. The Grashof number serves as an indicator of both the dimensionless Nusselt number and the ratio of buoyancy forces to viscous forces in the context of thermal transfer. In analyzing heat transfer processes, the Nusselt number stands out as a

 https://doi.org/10.5281/zenodo.14227176

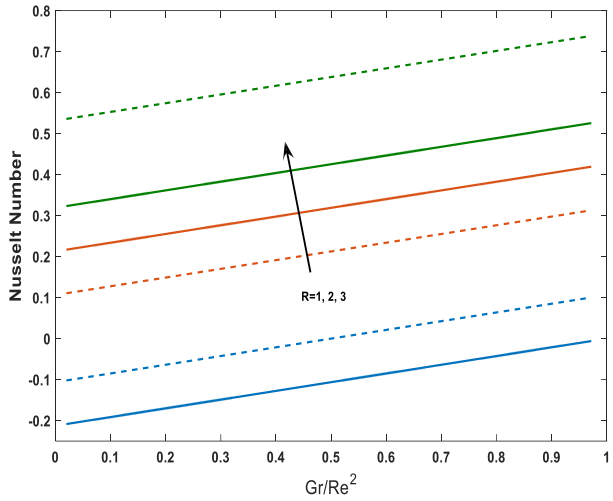

Figure 14: Nusselt number for various values of R

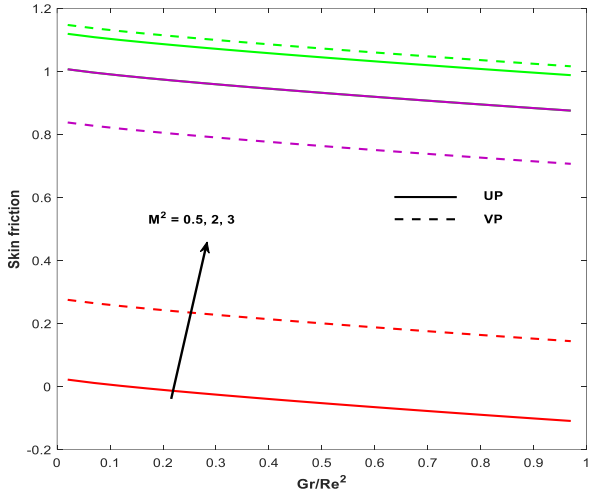

Figure 15: Skin friction for various values of M^2

vital measurement for both convective and conductive methods. A greater Nusselt number signifies that convective heat transfer dominates over conductive heat transfer. Across all examined radiation parameter values, the Nusselt number experiences an increase with the rise of the Grashof number. This phenomenon occurs due to the enhancement of buoyant forces, which promote fluid motion and consequently facilitate improved heat transfer, as the Grashof number escalates.

Table 2: Comparative analysis of $f''(0)$ and $-\theta'(0)$ for Pr= 0.71, E_c=0.1, ε_0=0.4, R=φ=0 in UP and VP cases :

M	$\frac{Gr}{\mathrm{Re}^2}$	β^*	Nalinakshi et al.[26]				Preset study			
			UP		VP		UP		VP	
			$f''(0)$	$-\theta'(0)$	$f''(0)$	$-\theta'(0)$	$f''(0)$	$-\theta'(0)$	$f''(0)$	$-\theta'(0)$
0.0	0.0	0.0	0.456893	0.300826	0.467886	0.396778	0.47100	0.31124	0.47768	0.46882
		0.1	0.570024	0.326784	0.573214	0.399978	0.57764	0.33589	0.57775	0.37640
		0.5	0.994532	0.456781	0.984919	0.524678	1.00561	0.46656	1.01456	0.53646
		0.9	1.304657	0.700567	1.294623	0.800321	1.39237	0.71522	1.39336	0.87645
	0.1	0.0	0.559087	0.299945	0.553608	0.386262	0.56984	0.30021	0.56981	0.37593
		0.1	0.679265	0.356782	0.682864	0.414960	0.69657	0.35996	0.69721	0.41456
		0.5	1.159872	0.713457	1.135678	0.800032	1.15782	0.71784	1.15812	0.82341
		0.9	1.364879	0.800267	1.354657	0.834567	1.36645	0.82678	1.36631	0.83467
	0.2	0.0	0.668432	0.302458	0.685034	0.396120	0.67658	0.31467	0.67714	0.39920
		0.1	0.784567	0.306892	0.793051	0.399673	0.78867	0.31567	0.78876	0.39673
	2.0	0.1	2.264556	0.425674	2.262345	0.419082	2.28690	0.42567	2.28867	0.42790
1.0	0.2	0.0	0.965478	0.356912	0.976456	0.394134	0.96878	0.36690	0.97645	0.39513
		0.1	1.231065	0.367823	1.237803	0.400345	1.34567	0.37823	1.23880	0.440345
		0.5	1.481910	0.398795	2.331602	0.445354	1.49835	0.39996	1.99478	0.46530
	2.0	0.1	2.321546	0.456321	1.003782	0.413678	2.33154	0.46782	2.33023	0.43678
5.0	0.2	0.0	1.358431	0.415678	1.365432	0.435216	1.35754	0.41678	1.45692	0.45216
		0.1	1.454890	0.427856	1.465390	0.446782	1.43677	0.43762	1.48021	0.44682
		0.5	1.668054	0.448961	1.689042	0.458653	1.88980	0.45234	1.95617	0.45653
	2.0	0.1	2.435765	0.426718	2.446790	0.435673	3.21031	0.43681	3.45891	0.45673

https://doi.org/10.5281/zenodo.14227176

From Figure 16, an augmentation in M^2 and Gr/Re^2 results in enhanced skin friction attributable to a synergistic effect of magnetic and buoyancy forces. An escalation in magnetic parameters alongside Gr/Re^2 culminates in elevated Lorentz and buoyancy forces acting upon the fluid. As M^2 and Gr/Re^2 escalate, a marked increase in skin friction is observed.

The juxtaposition is illustrated in Table 2, where the alignment of the model's outcomes to five decimal points confirms validity in the lack of radiation and volume fraction.

5. CONCLUSION

1. The velocity profile reduces with increasing solid volume fraction, heat absorption and magnetic parameter but the opposite trend is observed in the temperature profile with increasing volume fraction, and heat generation as observed in both UP and VP cases.
2. An increase in the value of the buoyancy parameter Gr/Re^2 leads to an increase in the velocity closer to the plate for both UP and VP cases, whereas VP is dominated by UP, which also decreases the temperature profiles for VP and UP.
3. The Nusselt number increases with the Grashof number for all radiation parameter values due to enhanced buoyancy-driven convective heat transfer.
4. The velocity profile increases in the order of the nanofluids Ag-water, Cu-water, and CuO-water in the VP case.
5. The Grashof number, a measure of thermal transfer, influences the Nusselt number and buoyancy forces, with a higher Grashof number indicating convective heat transfer.
6. The increase in magnetic parameters and Gr/Re^2 leads to increased skin friction due to the synergistic effect of magnetic and buoyancy forces.

REFERENCES

[1] Choi S.U.S., "Enhanced thermal conductivity of nanofluids with nanoparticles, development and applications of Newtonian flow", FED vol. 231/MD-vol.66, pp. 99-105, 1995.

[2] Choi S. U. S, Zhang Z. G Yu W, Lockwood F. E, Grulke E. A., "Anomalous Thermal Conductivity Enhancement in Nanotube Suspensions", Applied Physics Letters, vol. 79, pp.2252, 2001.

[3] Wang H Y., Lee J K., Lee C H., Jung Y M., Cheong S I., Lee C G., Ku B C. & Jang S.P., "Stability and thermal conductivity characteristics of nanofluids", Thermochimica Acta, vol. 455(1), 70–74, 2007.

[4] Das S.K., Choi S U S., Yu W., & Pradeep T., "Nanofluids: Science and Technology", Wiley, New Jersey,2007.

[5] Kakac S., & Pramuanjaroenki A., "Review of convective heat transfer enhancement with nanofluids", International Journal of Heat and Mass Transfer, vol. 52, no. 13-14, pp. 3187-3196, 2009.

[6] Chandrasekar M, Suresh S, "A review on the mechanisms of heat transport in nanofluids", Heat Transfer Eng, vol. 30, pp. 1136–1150, 2019.

 https://doi.org/10.5281/zenodo.14227176

[7] Khanafer K., Vafai K., "A critical synthesis of thermophysical characteristics of nanofluids", International Journal of Heat and Mass Transfer, 54(19-20), 4410-4428, 2011.

[8] Gasser R.D., Kazimi M.S., "Onset of convection in a porous medium with internal heat generation", ASME J. Heat Transfer, Vol.98, pp. 49-54,1976.

[9] Moalem D., "Steady-state heat transfer within a porous medium with temperature-dependent generation", Int. J. Heat Mass Transfer, Vol.19, pp. 529-537, 1976.

[10] Vajravelu K., "Effects of variable properties and internal heat generation on natural convection at a heated vertical plate in the air", Numerical Heat Transfer, Vol. 3, no. 3, 345-356, 1980.

[11] Makinde O. D., & Aziz A., "Boundary layer flow of a nanofluid past a stretching sheet with a convective boundary condition", International Journal of Thermal Sciences, vol. 49, no.9, pp.1813-1820, 2010. doi: 10.1016/j.ijthermalsci.2010.05.015.

[12] Chandrasekhara B. C., & Namboodiri P.M.S., "Influence of variable permeability on combined vertical surfaces in a porous medium", International Journal of Heat Mass Transfer, vol. 28, no.199-206. 1985.

[13] Olanrewaju P.O., Arulogun O.T., & Adebimpe K., "Internal heat generation effect on thermal boundary layer with a convective surface boundary condition", American Journal of Fluid Dynamics, Vol. 2, no. 1, pp. 1-4, 2012.

[14] Nalinakshi N., Dinesh P.A., & Chandrashekar D.V., "Effects of internal heat generation and variable fluid properties on mixed convection past a vertical heated plate", Fluid Dynamics and Material Processing, Vol. 10, pp. 465-490, 2014.

[15] Nalinakshi N., Dinesh P.A., & Chandrashekar D.V., "Shooting method to study mixed convection past a vertical heated plate with variable fluid properties and internal heat generation", Mapana J. Sci., Vol.13, pp. 31-50, 2014.

[16] Buongiorno J., Hu W., **"**Nanofluid heat transfer enhancement for nuclear reactor applications", Proceedings of ICAPP, vol. 5, 1192-1200, 2005**.**

[17] Sheikholeslami M., Ganji D. D., & Ghasemi B., "MHD mixed convection boundary layer flow over a vertical plate with internal heat generation and thermal radiation effects", International Journal of Thermal Sciences, 68, 830-840, 2013.

[18] Sheikholeslami M., & Shafii M., "MHD nanofluid flow and heat transfer over a vertical plate with internal heat generation in the presence of a chemical reaction and thermal radiation", Energy Conversion and Management, vol. 80, pp. 178-188, 2014. doi: 10.1016/j.enconman.2014.

[19] Krishna Hari., Anupama Yaragani., Vijaya Anumolu., Lakshmi G., Bindu Pathuri., & G.V.R. Reddy., "Heat and Mass Transfer Effects on MHD Mixed Convective Flow of a Vertical Porous Surface in the Presence of Ohmic Heating and Viscous Dissipation", CFD Letters, vol. 16, no.12, pp. 72–84, 2024. DOI: 10.37934/cfdl.16.12.7284.

[20] Padma S. V., Mallesh M. P., Shankar Rao Munjam., & Kottakkaran Sooppy Nisar, "Time-dependent MHD Free convective heat circulation of hybrid nano liquid over a vertical Porous Plate due to temperature oscillation with thermal radiation and viscous dissipation",

Advanced Research in Fluid Mechanics and Thermal Sciences, vol. 111, no. 2, pp. 65-85, 2023. doi: 10.37934/arfmts.111.2.6585.

[21] Xiao Xin A., Masthanaiah A., Rushikesava Nainaru Tarakaramu, Sherzod Abdullaev M., Khan M. I., Imen Rashid Bouazzi, "Magnetic field and dissipation effects on mixed convection viscous fluid flow by a channel in the presence of porous medium and heat generation/absorption phenomenon", Applied mathematics and mechanics, vol. 104, no. 2, 2024. DOI: 10.1002/zamm.202300625.

[22] Matao P. M., Reddy B. P., & Sunzu J. M., "Hall and viscous dissipation effects on mixed convective MHD heat absorbing flow due to an impulsively moving vertical porous plate with ramped surface temperature and concentration", vol. 104, no. 5, 2024. doi: 10.1002/zamm.202300210.

[23] Basant K. Jha & Gabriel Samaila, "Mixed convection flow from a convectively heated vertical porous plate with combined effects of suction/injection, internal heat generation and nonlinear thermal radiation", Proceedings of The Institution of Mechanical Engineers, Part E: Journal Of Process Mechanical Engineering, vol. 237, vol. 4,2022. DOI: 10.1177/09544089221116963.

[24] Basant K. Jha & Gabriel Samaila, "Nonlinear approximation for buoyancy-driven mixed convection heat and mass transfer flow over an inclined porous plate with Joule heating, nonlinear thermal radiation, viscous dissipation, and thermophoresis effects", Numerical Heat Transfer Part B-fundamentals, vol. 83, no. 4, pp. 139-161, 2022 doi: 10.1080/10407790.2022.2150341.

[25] Madhura K. R., Babitha S., & Sitharama Iyengar, "Impact of heat and mass transfer on the mixed convective flow of nanofluid through a porous medium", International Journal of Applied and Computational Mathematics, vol. 3, no. 1, pp. 1361–1384, 2017. DOI: 10.1007/S40819-017-0424-3.

[26] Nalinakshi N., Dinesh P.A., and Chandrashekar D.V., "Effects of Variable Fluid Properties and MHD on Mixed Convection Heat Transfer from a Vertical Heated Plate Embedded in a Sparsely Packed Porous Medium", IOSR Journal of Mathematics, vol.7(1), 20-31,2013. DOI: 10.9790/5728-0712031

[27] Choi S. U. S, Zhang Z. G Yu W, Lockwood F. E, Grulke E. A. Anomalous Thermal Conductivity Enhancement in Nanotube Suspensions. Applied Physics Letters, vol. 79, pp.2252, 2001.

[28] Sheikholeslami M., & Rokni H. B., "Thermal radiation effect on mixed convection heat transfer of Al2O3-water nanofluid over a vertical plate with exponential porosity", Journal of Thermal Analysis and Calorimetry, *vol. 142*, no. 2, pp. 1143-1152, 2020. doi:10.1007/s10973-020-09269-0.

[29] Mohammadein A.A. and El-Shaer N.A., "Influence of variable permeability on combined free and forced convection flow past a semi-infinite vertical plate in a saturated porous medium", Heat Mass Transfer, vol.40, 341-346, 2004. doi: 10.1007/s00231-003-0430-3.

[30] Sravan Kumar T., Dinesh P. A., and Makinde O. D., “Impact of Lorentz Force and Viscous Dissipation on Unsteady Nanofluid Convection Flow over an Exponentially Moving Vertical Plate,” Mathematical Models and Computer Simulations, vol. 12, no. 4, pp. 631–646, Jul. 2020, doi: 10.1134/s2070048220040110.

[31] Aydin O., Kavya A., “Mixed convection of a viscous dissipating fluid about a vertical flat plate”, Applied Mathematical Modelling, vol. 31, pp. 843-853, 2007. doi: 10.1016/j.apm.2005.12.015.

[32] Rana P., Bhargava R., “Numerical study of heat transfer enhancement in mixed convection flow along a vertical plate with a heat source/sink utilizing nanofluids”, communication nonlinear science numerical simulation, communication nonlinear science numerical simulation, vol.16, pp.4318-4334, 2011. doi: 10.1016/j.cnsns.2011.03.014.